applied sciences

MDPI

Article

The Hidden Short-Term Electro-Thermal–Optical Feedback Loop in Circuit-Level Modeling of PV Hot-Spots

Marco Balato [1], Carlo Petrarca [1], Martina Botti [2,3,*], Antonio Pio Catalano [1], Massimo Vitelli [2], Luigi Costanzo [2], Luigi Verolino [1] and Dario Assante [4]

[1] Department of Electrical Engineering and Information Technologies, University of Naples Federico II, 80125 Naples, Italy; marco.balato@unina.it (M.B.); petrarca@unina.it (C.P.); antoniopio.catalano@unina.it (A.P.C.); verolino@unina.it (L.V.)
[2] Department of Engineering, Università degli Studi della Campania "Luigi Vanvitelli", 81031 Aversa, Italy; massimo.vitelli@unicampania.it (M.V.); luigi.costanzo@unicampania.it (L.C.)
[3] Department of Information Engineering, Electrical Engineering and Applied Mathematics, University of Salerno, 84084 Fisciano, Italy
[4] Faculty of Engineering, International Telematic University Uninettuno, 00186 Rome, Italy; d.assante@uninettuno.it
* Correspondence: mbotti@unisa.it

Abstract

Hot-spots represent a significant failure mechanism in photovoltaic (PV) modules, typically attributable to electrical mismatching. However, thermo-optical degradation of the encapsulant, including discoloration and delamination, can both trigger and amplify mismatch by inducing localized optical losses and temperature rise. The present paper proposes a compact circuit-level electro-thermal–optical model that explicitly captures the short-term closed-loop interaction between mismatching, cell temperature, and temperature-dependent optical properties. The photogenerated current is formulated as a function of irradiance, cell temperature, and encapsulant degradation, enabling dynamic feedback between heating and optical losses. Numerical simulations are carried out on a commercial 40-cell PV module under four representative operating static scenarios. The results demonstrate that, even in the absence of shading, optical degradation can generate multimodal P–V characteristics, drive cells into reverse bias, and produce hot-spots. When optical degradation coexists with irradiance mismatch, the feedback loop significantly amplifies mismatching and shifts the maximum power point toward thermally unsafe operating conditions. These findings demonstrate that maximizing instantaneous power does not necessarily maximize lifetime energy yield, underscoring the need for thermal-aware MPPT strategies and providing a practical framework for early detection of thermo-optical faults in PV modules.

Keywords: mismatching; optical degradation; electro-thermal model

Academic Editor: Ephraim Suhir

Received: 4 January 2026
Revised: 29 January 2026
Accepted: 30 January 2026
Published: 3 February 2026

1. Introduction

Hot-spots represent one of the most critical failure modes in photovoltaic (PV) modules, arising from nonuniform electrical and thermal operating conditions across cells or modules [1,2]. Localized temperature peaks exceed one hundred degrees Celsius [3], severely limiting energy yield and accelerating irreversible degradation processes that may culminate in thermal runaway or combustion [4–7]. Methods proposed in the literature with the aim of mitigating hot-spots are, essentially, the adoption of bypass diodes, reconfigurable architectures and distributed power electronics converters [7–9]. Traditionally,

hot-spots have been interpreted as the direct consequence of mismatching phenomena, such as partial shading, manufacturing tolerances, or soiling.

Recent studies indicate that this relationship is inherently bidirectional: while mismatching can trigger local heating, the resulting thermal stresses can in turn accelerate degradation mechanisms that further intensify the mismatch. This interplay reveals an intrinsic closed-loop interaction between electrical mismatch, thermal behavior, and aging phenomena [4]. While the closed-loop relationship between mismatch and aging has been theoretically discussed in the literature [4], there is the need for a compact circuit-level formulation, useful for numerical analysis, of such a bidirectional relationship.

Among the degradation processes contributing to this feedback loop, thermo-optical degradation such as encapsulant discoloration and delamination plays a particularly influential role. As delineated in Section 2, degradation of the encapsulant manifests through reduced optical transmittance, increased diffuse reflection, and enhanced cell heating [10–14]. Experimental evidence shows that these thermo-optical mechanisms are themselves strongly temperature-dependent and can be triggered or intensified by local hot-spots, establishing a self-reinforcing cycle between mismatch, temperature rise, and optical losses [15–18]. Despite its clear physical basis, this closed-loop thermo-optical pathway has not yet been explicitly incorporated into compact PV models suitable for circuit-level simulation. Addressing this gap requires a framework capable of connecting electrical, thermal, and optical domains without resorting to computationally expensive multi-physics simulations. In this context, electro-thermal modeling of PV sources has been extensively investigated, particularly in relation to hot-spot formation and mismatch conditions. Existing studies can be broadly classified into three main categories. The first category includes several circuit-based electro-thermal models that analyze temperature–current coupling and hot-spot behavior under partial shading or electrical nonuniformities, while neglecting degradation effects and assuming constant photovoltaic cell properties [18,19]. The second category includes open-loop degradation-oriented electro-thermal studies that investigate the electrical impact of encapsulant discoloration or optical losses by introducing degradation as a static or externally imposed parameter, without dynamically coupling temperature, degradation evolution, and electrical mismatch [20,21]. Finally, the third category contains non-circuit-based approaches, including optical, thermal, or multi-physics finite-element models. They provide detailed insight into localized degradation phenomena and hot-spot temperatures but are not readily applicable to system-level electro-thermal simulations due to their computational complexity [12,22–24]. Overall, while electro-thermal modeling and degradation analysis are both well established in the prior literature, the explicit integration of temperature-dependent optical parameters within a closed-loop electro-thermal–optical circuit framework remains unexplored. In [20] an open-loop electro-thermal–optical circuit model is proposed, in which encapsulant reflectance was treated as a fixed parameter. In this paper, an electro-thermal–optical circuit-level model is proposed which is able to capture the closed-loop interaction whereby mismatch leads to hot-spot formation and the associated temperature rise induces the variation in the optical properties. As is detailed in Section 2, the resulting temperature-dependent variations in reflectance and transmittance exacerbate the current mismatch. In particular, as discussed in Section 3, a temperature-dependent representation of encapsulant reflectance and transmittance is integrated into the electro-thermal formulation proposed in [18]. In this way, the photogenerated current I_{ph} becomes sensitive not only to irradiance and cell temperature but also to the optical parameters of the encapsulant. As a result, the proposed model dynamically captures the reinforcing feedback between local heating, optical property variations and current mismatch, providing a physically grounded tool to evaluate how hot-spot formation influences optical properties and overall system performance. It is worth noting that various materials

can be used as encapsulants for PV modules, such as EVA (Ethylene–Vinyl Acetate), POE (Polyolefin Elastomer) and PVB (Polyvinyl Butyral). The model proposed in this paper is valid regardless of the specific encapsulant material adopted even if the following analysis focuses on the case of EVA, which is the most widely used encapsulant material in photovoltaic modules.

The remainder of this paper is organized as follows: Section 2 reviews the physical mechanisms underlying thermo-optical degradation and highlights the experimental evidence supporting the existence of the closed-loop interaction. Section 3 presents the proposed electro-thermal circuit model and its formulation of the temperature-dependent optical parameters. Section 4 reports the numerical simulations carried out under representative mismatch scenarios, including the impact of bypass diodes. Section 5 concludes the work.

2. Electro-Thermal–Optical Degradation and the Emerging Closed-Loop Mechanism

Discoloration and delamination have been identified as prevalent degradation phenomena in field-exposed PV modules, with substantial implications for the optical behavior of the EVA encapsulant. Prolonged UV exposure and elevated operating temperatures initiate photooxidative reactions that modify the polymer structure. These reactions subsequently lead to the formation of chromophoric groups and acetic acid [10–12]. These alterations, however, compromise the transparency of the encapsulant, thereby augmenting diffuse reflection and, consequently, diminishing the photogenerated current. Acetic acid has also been shown to weaken the adhesion between layers, thereby facilitating delamination at the EVA/glass and EVA/cell interfaces. This process is further promoted by humidity, mechanical stress, and UV radiation [10,13,14]. Delamination has been shown to enhance optical decoupling and local reflectance. This, in turn, has been demonstrated to raise the temperature of the affected region and accelerate cell degradation. Recent studies on environmental fatigue of EVA laminates have demonstrated that elevated temperatures (60–80 °C) and humidity levels promote the hydrolysis of vinyl acetate groups, resulting in morphological deterioration and interfacial delamination. This, in turn, leads to increased scattering and transparency loss [15]. The optical response of the encapsulant is also influenced by its degree of cross-linking: regions with insufficient or nonuniform curing exhibit higher diffuse reflectance, as demonstrated by Li et al. [16]. As EVA curing adheres to an Arrhenius-type temperature dependence, even modest thermal gradients—such as those engendered by mismatch or early hot-spot development—can give rise to spatial variations in reflectance and photocurrent generation. Further evidence suggests that discoloration can function as both a trigger and a consequence of mismatch-induced heating [17]. Collectively, these observations support the existence of an electro- thermal–optical feedback mechanism in which temperature rise, optical degradation, and electrical mismatch reinforce one another. As shown in Figure 1, mismatching in photovoltaic modules can have short-term and long-term effects, resulting in two closed feedback loops. In the following, with “short-term” we indicate time windows with durations (about 10 h) much smaller than the durations of the time windows typically adopted for carrying out accelerated aging tests (1000 h) [25]. With “long-term” we indicate time windows with durations comparable to the typical time constants of aging phenomena (much longer than 1000 h). Short-term effects of mismatching are basically associated with an increase in the temperature of the cell that impacts its optical properties, which in turn directly change the photogenerated current, thereby reinforcing mismatching and closing the short-term feedback loop. Long-term effects of mismatching are instead associated with the progress of optical degradation, which also affects the photogenerated current, closing the long-term feedback loop. In the

following, only the effects of the short-term feedback loop will be studied by focusing on the impact of mismatching on the cell temperature increase and the associated variation in optical properties (reflectance and transmittance). The optical degradation level will be considered fixed and externally imposed, since the study of the effect of the long-term feedback loop is not the subject of the present paper.

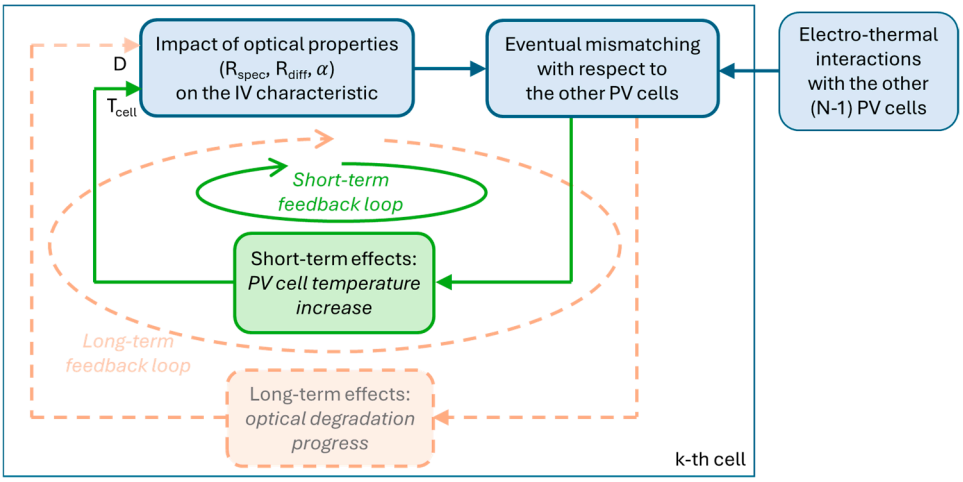

Figure 1. Conceptual representation of the double electro-thermal–optical feedback between electrical mismatch and performance degradation in photovoltaic modules.

3. Electro-Thermal–Optical Closed-Loop Circuit Model

Based on the above considerations, a compact electro-thermal model was developed to capture this bidirectional interaction and is described in this section. The proposed schematic circuit model of a PV cell, illustrating the closed-loop correlation between electrical mismatching and thermo-optical degradation, is shown in Figure 2.

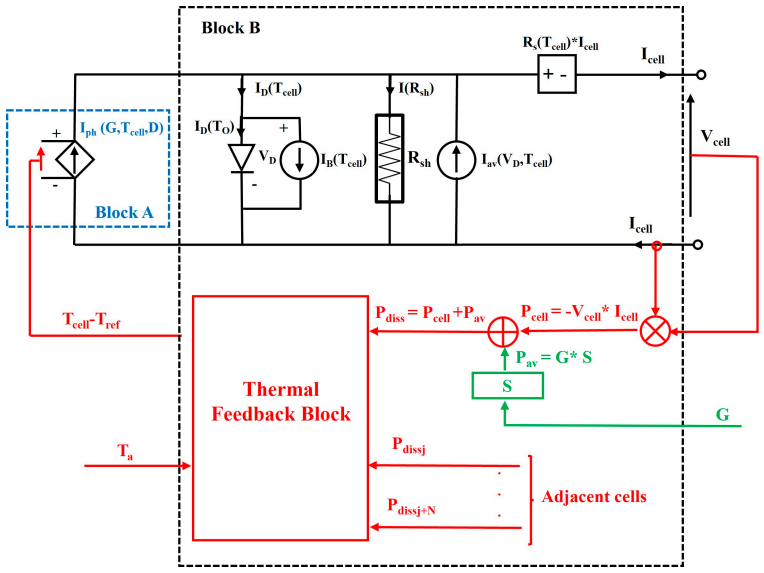

Figure 2. Schematic model for a PV cell taking into account the closed-loop link between mismatching and optical degradation.

The proposed model is based on the compact electro-thermal formulation by Guerriero et al. [18] and includes a thermal network that interacts dynamically with the electrical subcircuit. Each cell is modeled as a heat source, and its dissipated power (P_{diss}) is fed into a Thermal Feedback Block. This block evaluates the cell temperature by considering both

self-heating and thermal coupling with adjacent cells. The thermal network is generated from a full 3D discretization of the module structure and is reduced via a moment-matching procedure to a generalized Foster thermal model [18]. In this representation, the thermal resistances describe conductive heat transfer among the solar cells, while the thermal capacitances capture the dynamic response of the module. Convective and radiative exchanges at the front and rear surfaces establish the nonlinear boundary conditions that govern heat dissipation to the ambient environment. The main modification with respect to the electro-thermal formulation by Guerriero et al. [18] concerns the reformulation of the photogenerated current I_{ph} (Block A), which is now expressed as a function of the irradiance G, the PV cell temperature T_{cell}, and the encapsulant's optical degradation level D (with $D \in [0, 1]$).

Regarding Block A, the adopted formulation for I_{ph} is

$$I_{ph}(G, T_{cell}, D) = \frac{J_{sc}(T_{cell}, D) \cdot S \cdot G}{G_{STC}} \quad (1)$$

where J_{sc} is the short-circuit current density (A/cm^2), S is the PV cell area (cm^2), and G is the incident irradiance (W/m^2). This equation is normalized with respect to the Standard Test Conditions (STCs), which correspond to an AM1.5 spectral distribution, an ambient temperature of 25 °C, and an irradiance of G_{STC} = 1000 W/m^2. In this formulation, a well-established analytical semiconductor model [26] is employed to express the short-circuit current density as a function of reflectance R, which depends on the PV cell temperature. Consequently, closed-loop behavior arises from the temperature-dependent variation in these optical properties. These properties then modulate the photogenerated current. In particular:

$$J_{sc}(T_{cell}, D) = \int_0^\infty [J_{scE}(\lambda, T_{cell}, D) + J_{scB}(\lambda, T_{cell}, D)] d\lambda \quad (2)$$

where J_{scE} (J_{scB}) is the emitter (base) short-circuit spectral current density, whose values are calculated using Equations (3) and (4).

$$J_{scE}(\lambda, T_{cell}, D) = q\phi_0[1 - R(T_{cell}, D)]\alpha L_P(\alpha L_P - 1)\left[\frac{\alpha L_P e^{-\alpha W_e}\frac{S_e L_p}{D_p} + \left(\alpha L_P - e^{-\alpha W_e}\right)\frac{S_b W_e}{D_p}}{\frac{S_e L_p}{D_p} + \frac{S_b W_e}{D_p} + \alpha L_P}\right] \quad (3)$$

$$J_{scB}(\lambda, T_{cell}, D) = q\phi_0\, e^{-\alpha W_e}[1 - R(T_{cell}, D)]\alpha L_n(\alpha L_n - 1)\left[\frac{\alpha L_n e^{-\alpha W_b}\frac{S_b W_b}{D_n} + \left(\alpha L_n e^{-\alpha W_b}\right)\frac{S_e L_n}{D_n}}{\frac{S_b L_n}{D_n} + \frac{S_b W_b}{D_n} + \alpha L_n}\right] \quad (4)$$

where $\phi_0(\lambda) = 10^{16} I_\lambda \cdot \lambda / 19.8$ (I_λ is the spectral irradiance [$W/m^2\mu m$]) [26]. All symbols used in Equations (3) and (4) are defined in Table 1. As detailed in the following section, these values can be obtained after characterizing the PV cell using PC1D software (PC1D is the commonly used software to simulate PV cells) [27]. Using these parameters, the circuit model in Figure 2 can be simulated in any circuital simulation environment like Altair PSIM. Additional information regarding Block B is provided in [18]. It is worth noting that the absorption coefficient α is treated as constant in the present formulation. Although the absorption of crystalline silicon exhibits a temperature dependence, particularly near the band edge, its contribution to the integrated short-circuit current is limited. For short-term electro-thermal simulations, temperature-induced variations in reflectance and scattering, primarily associated with encapsulant degradation, dominate the thermo-optical response. As shown by Schinke et al. (2015) [28], the impact of temperature-dependent absorption on photovoltaic performance is minor compared to other optical loss mechanisms. Accordingly,

neglecting $\alpha(\lambda,T_{cell})$ represents a deliberate modeling simplification that preserves the dominant feedback mechanisms.

Table 1. Main parameters involved in the analytical model of the PV cell.

Symbol	Name	Units	Values
α	Absorption coefficient	cm^{-1}	1.6×10^{-19}
q	Electron charge	C	1.6×10^{-19}
L_n	Electron diffusion length (base)	cm	0.0162
L_P	Hole diffusion length (emitter)	cm	4.3×10^{-6}
D_n	Electron diffusion constant	cm^2/s	36.33
D_p	Hole diffusion constant	cm^2/s	3.4
S_e	Emitter surface recombination	cm/s	36.3
S_b	Base surface recombination	cm/s	2×10^4
W_e	Emitter thickness	cm	0.03
W_b	Base thickness	cm	0.03
λ	Wavelength	µm	[0.3–1.2]

In the present formulation, the reflectance of the PV cell is modeled as the sum of a constant specular term and a diffuse term that depends on temperature:

$$R(T_{cell}, D) = R_{spec} + R_{diff}(T_{cell}, D) \quad (5)$$

where R_{spec} represents the specular reflectance at the air–EVA interface, assumed invariant with temperature, and estimated using the Fresnel equation at normal incidence:

$$R_{spec} = \left(\frac{n-1}{n+1}\right)^2 \quad (6)$$

At normal incidence, the refractive index (n) of the glass–EVA encapsulant was set to n = 1.50 (λ = 550 nm), corresponding to a specular reflectance $R_{spec} \approx 0.04$. This value is consistent with experimentally measured optical constants of conventional EVA reported by Mcintosh et al. [29] and confirmed by subsequent optical simulations of encapsulated cells [30]. Diffuse reflectance R_{diff} accounts for the scattering effects caused by degradation, including haze and surface roughness. It is modeled as an exponential function of temperature and degradation:

$$R_{diff}(T_{cell}, D) = R_0 + k_0 \cdot D \cdot e^{[\beta \cdot (T_{cell} - T_{ref})]} \quad (7)$$

Regarding the degradation parameter D, it is treated as fixed in the present formulation, such that only the temperature dependence is dynamically considered. This assumption reflects the quasi-static nature of material degradation, which evolves over timescales much longer than thermal fluctuations. As a result, the following analysis isolates the short-term thermo-optical response of the encapsulant from long-term aging kinetics.

The reference temperature was set to T_{ref} = 26.85 °C (300 K), in accordance with [18].

The parameters R_0 (R_0 = 0.0177), k_0 (k_0 = 0.36) and β (β = 3.33 × 10^{-3} K^{-1}) were determined by imposing that the behavior of the normalized photogenerated current at a cell temperature of 25 °C, as a function of D, is in good agreement with the findings reported in [21], as is shown in Figure 3a. In particular, in [21], four different encapsulant degradation levels, namely yellow-brown 1, yellow-brown 2, brown, and dark brown, were considered, corresponding to variations in the photogenerated current ranging from approximately 59% to 93% with respect to the unexposed scenario. In the present model, the values of the degradation parameter D reproducing the scenarios reported in [21] are D = 0

(unexposed encapsulant), D = 0.15 (yellow-brown 1), D = 0.17 (yellow-brown 2), D = 0.58 (brown), and D = 0.98 (dark brown). The adopted values of k_0, β, and T_{ref} ensure that the model reproduces realistic short-term variations in optical losses within the usual PV cell operating range. Equation (7) is thus designed to delineate diffuse reflectance fluctuations exclusively within the conventional operational temperature range of photovoltaic modules ($T_{cell} \leq 100$ °C). This simplified structure allows a direct coupling between the thermal and electrical domains: when mismatch conditions arise, local heating develops, leading to a nonuniform increase in R (T_{cell}, D). This temperature-driven increase in reflectance reduces the locally generated photocurrent, thereby exacerbating the nonuniformity of current distribution across the PV cell. The resulting current mismatch, in turn, causes further localized heating, establishing closed-loop electro-thermal–optical feedback. It should be emphasized that this compact formulation neglects two important aspects that can be included in more complete models:

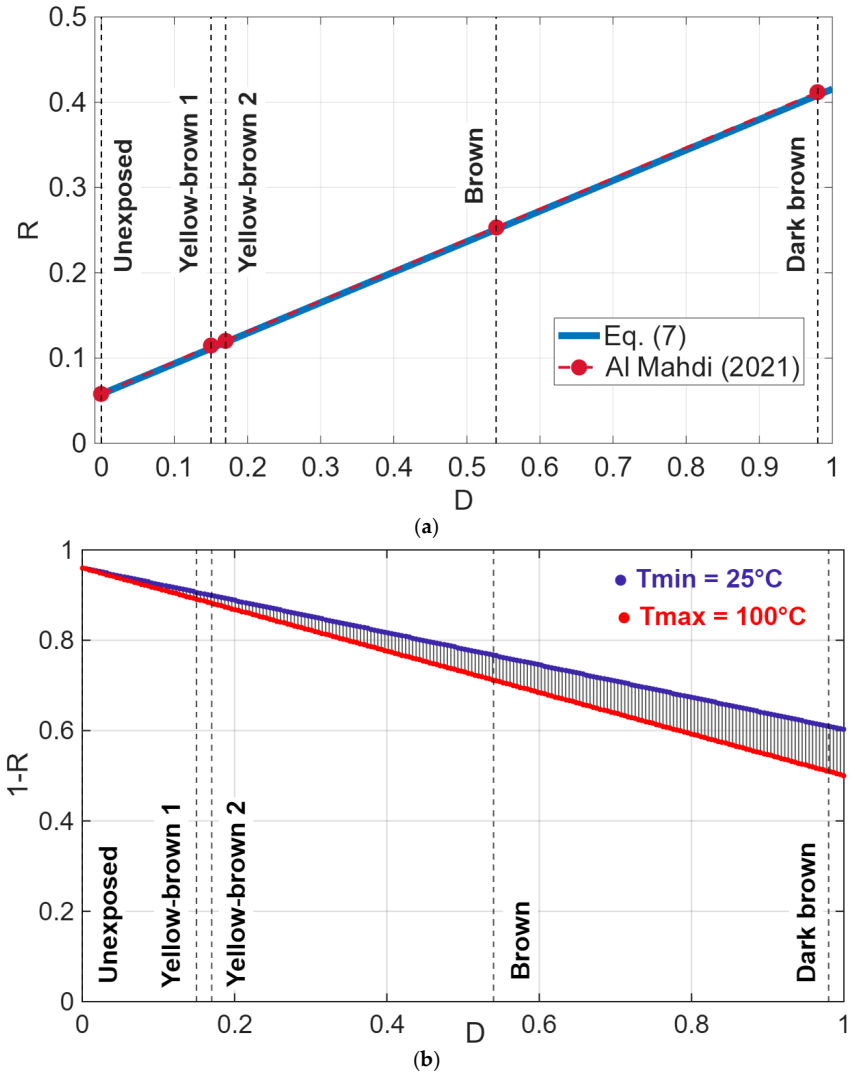

Figure 3. (**a**) Reflectance R(T_{cell}, D) versus encapsulant degradation level *D*; comparison with the experimental data in [21] (T_{cell} = 25 °C). (**b**) Normalized photogenerated current [1 − R (T_{cell}, D)] versus encapsulant degradation level *D*. Vertical segments indicate the range spanned over the investigated temperature interval (25–100 °C), while colored markers denote the minimum and maximum temperatures. Dashed lines mark experimentally relevant degradation states, highlighting that temperature increasingly amplifies photocurrent losses at advanced degradation levels.

(i) The spectral dependence of reflectance and encapsulant yellowing, which is known to penalize short wavelengths more strongly [31]; including spectral factors would increase the model's accuracy for different types of optical degradation.

(ii) The time- and stress-dependent kinetics of degradation, which govern the irreversible growth of scattering losses under prolonged UV exposure and high temperature [11,31].

By ignoring these contributions, the present model does not aim at predicting long-term optical aging but rather at highlighting the underlying principle of the closed-loop mechanism. Within this scope, the specular diffuse decomposition provides a sufficiently accurate approximation for short-term electro-thermal simulations, where the key phenomenon of interest is the emergence of a nonuniform photocurrent as the direct consequence of nonuniform heating and its feedback on mismatch. Figure 3 reproduces the result of the proposed optical degradation model.

The combined effect of encapsulant optical degradation and operating temperature on the normalized photogenerated current [1 − R (T_{cell}, D)] is illustrated in Figure 3b. The degradation level D is reported on the horizontal axis, while the vertical axis shows the normalized photogenerated current. For each value of D, the vertical segment represents the range of the quantity [1 − R (T_{cell}, D)] over the investigated temperature interval (25–100 °C), providing a direct measure of the temperature sensitivity at fixed degradation.

In order to circumvent any potential ambiguity in the graphical encoding, the temperature is exclusively indicated by the colored markers located at the extremities of the segments. This approach is consistent with the utilization of the side color bar. Conversely, the vertical segments are depicted in a neutral color. Dashed vertical lines are used to denote experimentally relevant degradation states of the encapsulant, thereby enabling a direct comparison between the model and real aging conditions. The figure evidently demonstrates that encapsulant degradation is a determining factor in the baseline loss in photogenerated current, with temperature acting as an amplifying factor. In the initial stages of degradation, the thermal effect remains negligible; however, as the degradation progresses, the same temperature excursion results in a substantial variation in [1 − R (T_{cell}, D)]. This underscores the profound interconnection between optical degradation and operating temperature. Furthermore, a sensitivity analysis has been carried out to show how parameter variations affect the value of reflectance. In particular, variations between −30% and +30% of the nominal values of k_0, β and T_{ref} have been considered. In Figure 4 the percentage variation in reflectance is shown. It is defined as

$$\Delta R = 100 \cdot \frac{R^* - R_{nom}}{R_{nom}} \quad (8)$$

where R* is the reflectance evaluated with a varied parameter, and R_{nom} is the reflectance evaluated with nominal parameters. The sensitivity analysis shows that variations in b and T_{ref} have a nearly negligible effect on R. The variations in k_0 are significantly larger than those in the other two parameters, making it a key parameter governing the model's behavior.

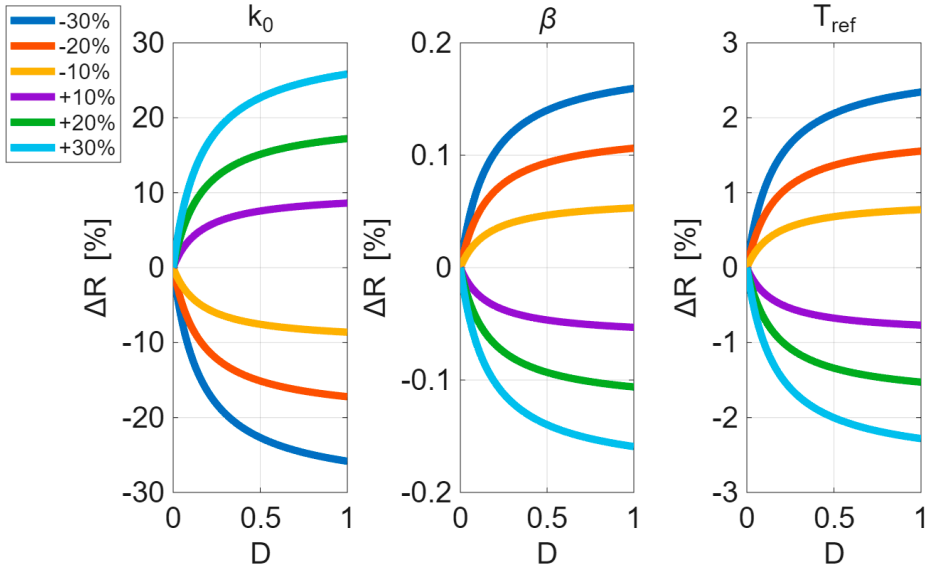

Figure 4. Percentage variation in R as a function of the variation in k_0, β and T_{ref} between −30% and +30% of nominal values (k_0 = 0.36, $\beta = 3.33 \times 10^{-3}$ K^{-1} and T_{ref} = 300 K).

4. Numerical Results

To assess the behavior of the proposed thermo-optical closed-loop model under realistic operating conditions, four representative scenarios were simulated using the commercial photovoltaic module ET-M54050A (ET Solar, Nanjing, Jiangsu, China). The geometric, electrical, and thermal parameters of the module are provided in [18] and summarized in Table 2.

Table 2. Main parameters of PV module.

Symbol	Name	Value
N	Number of cells	40
I_{sc}	Short-circuit current	2.8 A
I_{MPP}	Maximum power current	2.4 A
V_{MPP}	Maximum power voltage	20.2 V
V_{oc}	Open circuit voltage	24.6 V
NOCT	Normal Operating Cell Temperature	44.4 ± 2 °C
	Dimensions	719 × 555 × 34 mm

The module consists of two substrings of 20 mono-Si cells (Substring #1 and Substring #2), each protected by a bypass diode. In Figure 5, the adopted cell-numbering scheme and all simulated scenarios are presented (Case I, Case II, Case III and Case IV). In all simulations, the ambient temperature and wind speed were constant, thereby ensuring that any temperature variations originated exclusively from electrical or thermo-optical mechanisms.

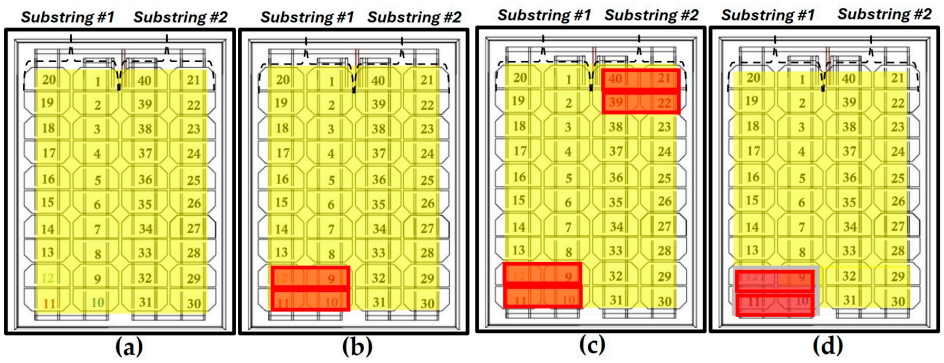

Figure 5. Schematic representation of the four operating conditions considered in the numerical analysis: (**a**) Case I—uniform irradiance with no optical degradation (reference condition); (**b**) Case II—uniform irradiance with a nonuniform thermo-optical fault affecting cells #9–12 (closed-loop model); (**c**) Case III—uniform irradiance with a uniform thermo-optical fault affecting cells #9–12, cells #21–22, and cells #39–40 (closed-loop model); and (**d**) Case IV—a nonuniform irradiance mismatch combined with a thermo-optical fault on cells #9–12 (closed-loop model).

On the basis of the semiconductor parameters obtained from PC1D simulations (Table 1), the photogenerated current I_{ph} (Block A) is formulated as follows:

$$I_{ph}(G, T_{cell}, D) = [1 - R(T_{cell}, D)] \cdot K \cdot G \quad (9)$$

where K is defined as the total short-circuit current, normalized to G_{STC}, evaluated under the assumption that R is equal to 0. The value of K, set at 2.94×10^{-3} A m^2/W, is derived from the total short-circuit current density, calculated by integrating the AM1.5 spectral contribution over wavelength. The integration is performed up to 1.2 µm [26].

It is noteworthy that, under STC (AM1.5 spectrum and G_{STC} = 1000 W/m^2) and in the absence of optical degradation (D = 0 and R = R_{spec} + R_0), Equation (9) reproduces the short-circuit current of the considered module (~2.8 A) [18]. This ensures consistency between the compact photocurrent formulation given by Equation (9) and the reference STC electrical characterization of the considered PV module.

Following the delineation of the term I_{ph}, the short-term closed-loop interaction between optical degradation mechanisms and hot-spots can be evaluated (see Figure 1). The present study was conducted to investigate the temperature distribution in the considered PV module under four distinct static scenarios. For the sake of clarity and without intending to limit the generalizability of the findings, it should be noted that only eight cells (designated as cells #9–12, cells # 21–22 and cells #39–40) were subjected to shading and/or optical degradation. Concurrently, the lateral heat-exchange network delineated in [18] was employed to ensure the preservation of thermal coupling with adjacent cells. Electrical characterization was performed through a voltage sweep that explicitly accounts for the thermal dynamics of the system. The thermal time constant is typically measured to be on the order of 400 s. Therefore, the time interval between successive perturbations in the sweep was established as 5τ~ = 2000 s. This ensured that each operating point reached its steady-state temperature before the next voltage step. Moreover, in the considered cases, the degradation level (D) is treated as a fixed parameter, since this study focuses on a short-term feedback loop. Although the degradation level increases as a consequence of the localized heating induced by the feedback loop, the associated time constants are much longer than the simulation times considered in this work [25].

4.1. Case I—Uniform Irradiance, No Degradation (Open-Loop)

All cells operate under standard test irradiance (G = 1000 W/m^2) with no optical degradation (D = 0). This case defines the electro-thermal reference condition of a healthy module. As demonstrated in Figure 6, which presents the resulting P–V characteristics in conjunction with the voltage-dependent temperature deviation of cells #9–12, the temperature field maintains a high degree of uniformity, thereby substantiating the absence of any mismatch-induced heating. The temperature profiles of the three cells differ by less than 5 °C, further indicating minimal thermal nonuniformity. It is also observed that the minimum temperature occurs at the maximum power point (MPP), consistent with the expected behavior of a module under optimal operating conditions.

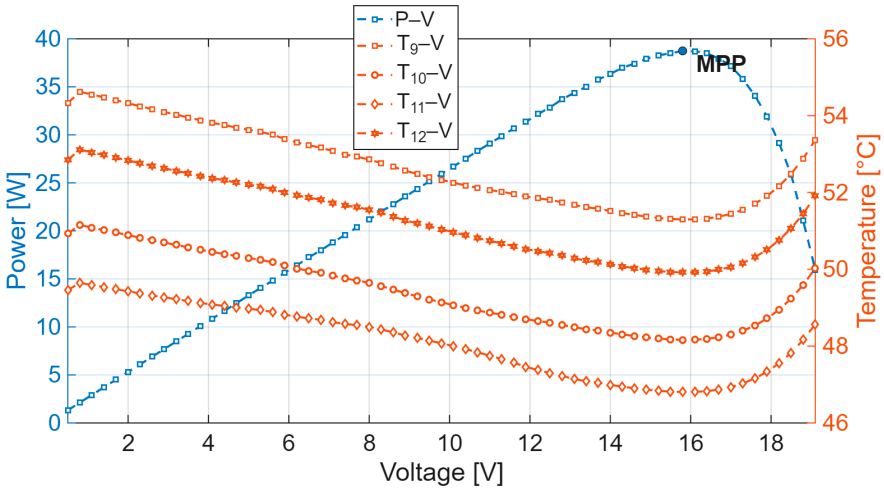

Figure 6. Power–voltage (P–V) characteristics and temperature–voltage (T–V) profiles of cells #9–12 for Case I—uniform irradiance and no optical degradation.

4.2. Case II—Uniform Irradiance with Thermo-Optical Fault (Closed-Loop)

The irradiance distribution is analogous to that of Case I; however, cells #9–12 are impacted by nonuniform encapsulant discoloration (D_9 = 0.58; D_{10} = 0.98; D_{11} = 0.17; D_{12} = 0.15) corresponding respectively to brown, dark brown, yellow-brown 2, and yellow-brown 1. Here, the short-term thermo-optical feedback is active: reflectance and, consequently, the photogenerated current vary with temperature. This configuration isolates the effect of local optical degradation, showing that discoloration alone can generate current nonuniformity and localized heating, even without external shading.

Figure 7 presents the resulting P–V characteristics. The reduced photogenerated current produced by the discolored cell in Case II drives the cells into reverse bias, thereby activating bypass diode #1. This transition gives rise to the characteristic multimodal shape of the P–V curve, highlighting how even localized optical degradation can substantially alter the power–voltage profile. The thermal implications of this mismatch are shown in Figure 8, which reports the T–V profiles for cell #10. In Case I, the temperature remains stable around 50–51 °C across the entire voltage range, reflecting uniform electrical loading. Conversely, Case II exhibits a substantial temperature rise once the cell enters reverse bias, ultimately exceeding 80 °C during bypass activation. The localized hot-spot is the result of increased dissipated power in the degraded cell. It is evident that the bypass activation voltage range is characterized by quite a high temperature profile and contains a relative MPP. It is well known that MPPT techniques can trap the operating point near a relative MPP, which, in Case II, is an operating condition to be avoided, since it is characterized by a waste of available power and at the same time by enhanced thermal stress with respect to the absolute MPP region. Upon the conclusion of the bypass interval, a subsequent decrease

in temperature is observed, which is consistent with the transition back to forward-bias operation. The results of the study demonstrate that encapsulant discoloration can induce substantial current nonuniformity and localized heating, even under uniform irradiation. This underscores the necessity of incorporating thermo-optical degradation mechanisms into assessments of module reliability and the propensity for hot-spot formation. To ensure comprehensive comparison, Figure 9 presents the temperature profiles of cells #9, #11 and #12 for both Case I and Case II.

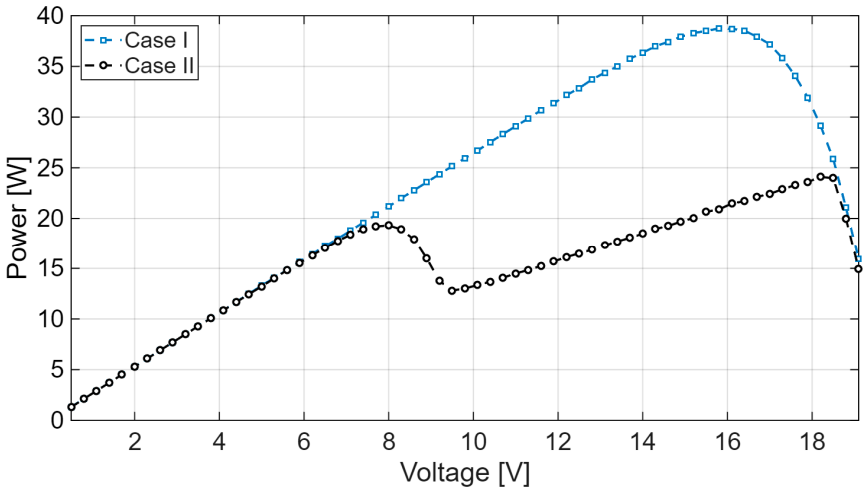

Figure 7. Power–voltage (P–V) characteristics for Case I and Case II.

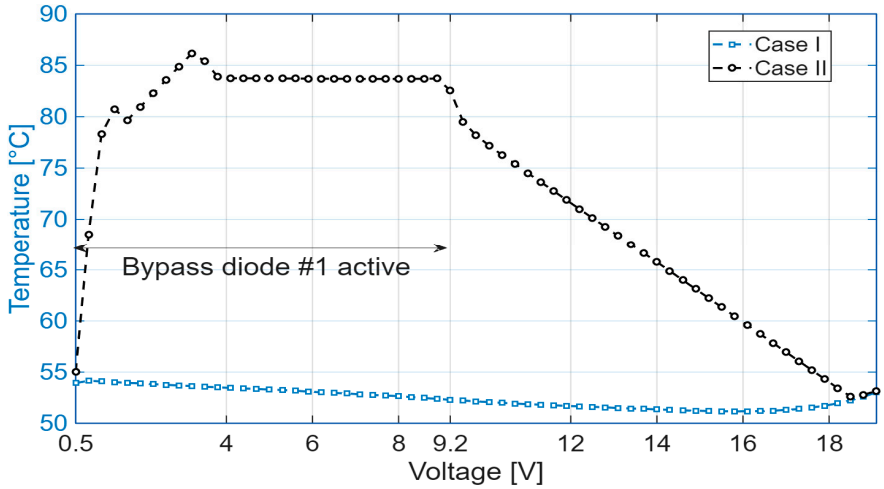

Figure 8. Temperature–voltage (T–V) profiles of cell #10 for Case I and Case II.

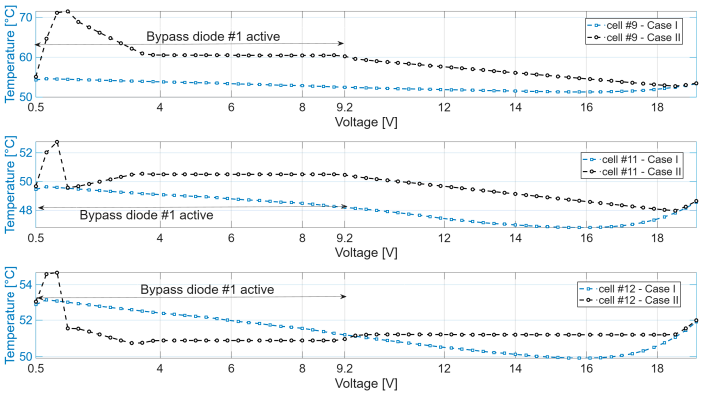

Figure 9. Temperature–voltage (T–V) profiles of cells #9, #11 and #12 for Case I and Case II.

4.3. Case III—Uniform Irradiance with a Thermo-Optical Fault (Closed-Loop) Without the Activation of Bypass Diodes

An additional scenario was analyzed to determine whether thermo-optical degradation can induce significant thermal nonuniformities even when the two substrings operate under the same conditions. In this configuration, the operating conditions are analogous to Case II; however, cells #9–12, cells #21–22, and cells #39–40 are impacted by nonuniform encapsulant discoloration ($D_9 = D_{39} = 0.58$; $D_{10} = D_{40} = 0.98$; $D_{11} = D_{21} = 0.17$; $D_{12} = D_{22} = 0.15$) corresponding respectively to brown, dark brown, yellow-brown 2, and yellow-brown 1. It is evident that, given each substring comprises four degraded cells, no bypass diode is activated. However, the simulation results presented in Figure 10 demonstrate a substantial increase in temperature within those cells demonstrating the most severe level of degradation (cells #10 and #40). This temperature increase, which occurs at the relative maximum power point (see Figure 10 vs. Figure 8), is analogous to the temperature increase observed in Case II. The maximum temperature attained in this instance is approximately 10 °C lower than in Case II, suggesting that the activation of the bypass diodes can be regarded as a significant factor contributing to the formation and intensification of hot-spots. Furthermore, this scenario offers a significant explanation for field cases in which hot-spots may occur despite the module's apparent operation under uniform irradiance and perfectly balanced electrical conditions (no activation of bypass diodes). Such situations often prove challenging to detect using conventional electrical measurements. If thermo-optical degradation is symmetrically distributed between the substrings, the electrical behavior of the module may not exhibit any classical mismatch indicators. However, localized heating may still develop due to the temperature-dependent reflectance of the degraded encapsulant. In such circumstances, the formation of hot-spots becomes an inherent aspect of the feedback loop between optical degradation, photocurrent reduction, and localized thermal rise, without necessitating an external mismatch to initiate the phenomenon.

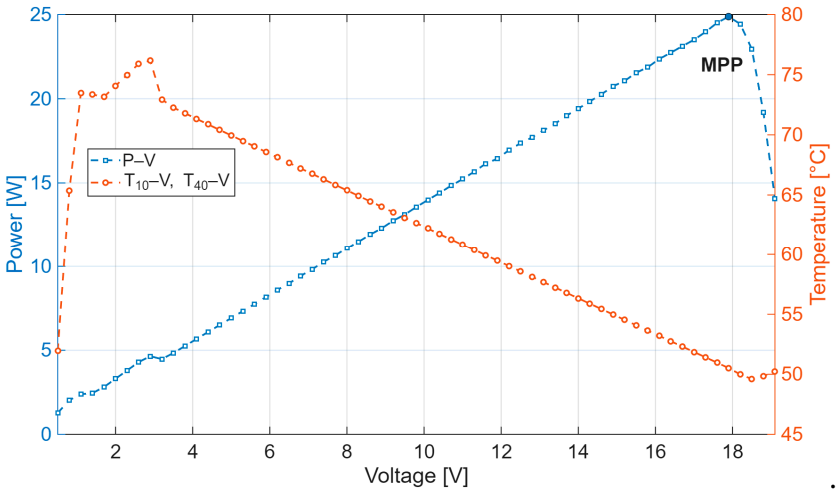

Figure 10. Power–voltage (P–V) characteristics and temperature–voltage (T–V) profiles of cells #10 and #40 for Case III.

4.4. Case IV—Irradiance Mismatch with Thermo-Optical Fault (Closed-Loop)

Cells #9–12 are exposed to nonuniform partial shading ($G_9 = 500\ W/m^2$, $G_{10} = 450\ W/m^2$, $G_{11} = 250\ W/m^2$, $G_{12} = 300\ W/m^2$), while all other cells within the module receive full irradiance ($G = 1000\ W/m^2$). However, these four cells now exhibit uniform encapsulant discoloration ($D_{9–12} = 0.58$), while the remaining cells exhibit $D = 0$. As demonstrated in Figure 11, the concurrence of optical degradation and irradiance mismatch gives rise

to a critical outcome: the absolute MPP is rather near to the point of maximum thermal stress for cell #12. In such conditions, it is preferable to get an operating point near the relative MPP (around 19 V) in order to substantially reduce thermal stress with respect to the absolute MPP at the price of wasting a negligible amount of energy. This is a pivotal observation, as it demonstrates that the electrically optimal operating condition may coincide with the thermally least secure one. This finding introduces new considerations for PV system operation and control. The conventional Maximum Power Point Tracking (MPPT) algorithms are engineered to ascertain the absolute MPP under any irradiance condition. However, when the MPP is thermally detrimental, the enforcement of instantaneous power maximization has the potential to accelerate module aging. This finding is consistent with well-established evidence linking elevated temperature to accelerated degradation. A multitude of degradation mechanisms, including encapsulant discoloration, bubble formation, EVA delamination, corrosion of metallic contacts, ribbon and solder fatigue, crack propagation, and failures of junction boxes or bypass diodes, are known to progress more rapidly under high thermal stress. Localized heating, whether caused by reverse-biased cells or bypass-diode conduction, is widely recognized as a leading contributor to premature field failures in PV generators. The present analysis further suggests that optical degradation, typically regarded as a long-term phenomenon, can also reshape the module's instantaneous electrical characteristics.

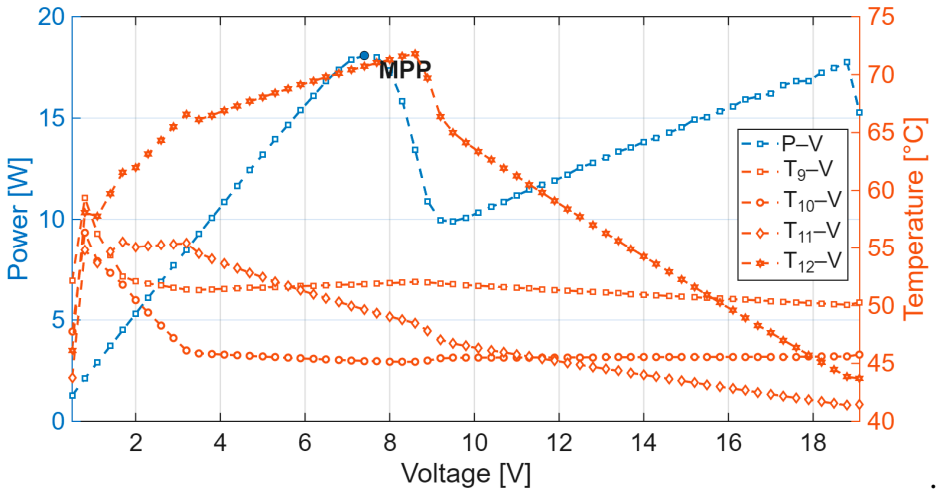

Figure 11. Power–voltage (P–V) characteristics and temperature–voltage (T–V) profiles of cells #9–12 for Case IV—irradiance mismatch with thermo-optical fault (closed-loop).

The above findings call for a more extensive revaluation of the traditional objective of optimizing instantaneous power. As indicated in previous PV system research, optimizing power output in the present does not necessarily translate into maximizing lifetime energy production [32,33]. The temperature distribution across different operating points is a critical factor in determining the degradation rates of the module. These degradation rates, in turn, influence the long-term reliability and performance of the module as a whole.

It is worth noting that the temperature levels and hot-spot magnitudes predicted in these simulations (Cases II, III and IV) are consistent with IR thermography measurements reported in the literature for field-aged PV modules affected by severe EVA discoloration, where localized hot-spots above 80–100 °C have been experimentally observed [34].

5. Conclusions

This work introduces a compact electro-thermal–optical model that incorporates, for the first time in a circuit-level formulation, the closed-loop interaction between electrical mismatch, temperature rise, and thermo-optical degradation of the encapsulant. Through

numerical simulations of a commercial PV module, obtained using the considered static conditions, we demonstrated that optical faults such as discoloration can generate multimodal P–V curves even in the absence of shading, thereby acting as intrinsic sources of mismatching. The model also reveals that the operating point corresponding to the maximum power may coincide with the maximum thermal stress on the degraded cell. This behavior becomes particularly severe when irradiance mismatch and thermo-optical degradation coexist, as the resulting feedback between heating and optical losses amplifies both electrical nonuniformity and hot-spot formation. These findings challenge the conventional assumption that maximizing instantaneous power always leads to optimal long-term performance. Instead, the results suggest that operating strategies should explicitly account for thermal safety and degradation dynamics. This perspective opens new opportunities to design future strategies for mitigating hot-spot issues, such as thermally aware MPPT algorithms, degradation-resilient PV configurations, and diagnostic tools capable of identifying early-stage optical faults. Future work will focus on extending the model to include spectral effects, irreversible degradation kinetics, and long-term aging behavior. Experimental validation under controlled mismatch and thermal conditions is in progress, with the aim to further strengthen the applicability of the proposed framework to real PV systems.

Author Contributions: Conceptualization, M.B. (Marco Balato), C.P. and M.V.; methodology, M.B. (Marco Balato), C.P. and M.V.; software, M.B. (Marco Balato), C.P. and M.B. (Martina Botti); validation, M.B. (Marco Balato), C.P. and M.B. (Martina Botti); formal analysis, M.B. (Marco Balato); investigation, M.B. (Marco Balato); resources, M.B. (Marco Balato); data curation, M.B. (Marco Balato); writing—original draft preparation, M.B. (Marco Balato), C.P., M.B. (Martina Botti), A.P.C., M.V. and L.C.; writing—review and editing, M.B. (Marco Balato), C.P., M.B. (Martina Botti), A.P.C., M.V., L.C., L.V. and D.A.; visualization, M.B. (Marco Balato), C.P., M.B. (Martina Botti), A.P.C., M.V., L.C., L.V. and D.A. All authors have read and agreed to the published version of the manuscript.

Funding: This research received no external funding.

Institutional Review Board Statement: Not applicable.

Informed Consent Statement: Not applicable.

Data Availability Statement: The original contributions presented in this study are included in the article. Further inquiries can be directed to the corresponding authors.

Conflicts of Interest: The authors declare no conflicts of interest.

References

1. García, M.; Marroyo, L.; Lorenzo, E.; Marcos, J.; Pérez, M. Observed degradation in photovoltaic plants affected by hot spots. *Prog. Photovolt. Res. Appl.* **2014**, *22*, 1292–1301. [CrossRef]
2. Ghosh, S.; Singh, S.K.; Yadav, V.K. Experimental investigation of hotspot phenomenon in PV arrays under mismatch conditions. *Sol. Energy* **2023**, *253*, 219–230. [CrossRef]
3. Amerasekera, A.; Chang, M.; Saatchi, M.; Chatterjee, J.; Mayaram, A.; Chern, J.H. Self-heating effects in basic semiconductor structures. *IEEE Trans. Electron. Devices* **1993**, *40*, 1836–1844. [CrossRef]
4. Manganiello, P.; Balato, M.; Vitelli, M. A survey on mismatching and aging of PV modules: The closed loop. *IEEE Trans. Ind. Electron.* **2015**, *62*, 7276–7286. [CrossRef]
5. Mahamudul, H.; Rahman, M.; Metselaar, M.; Mekhilef, H.; Shezan, S.; Sohel, R.S. Temperature regulation of photovoltaic module using phase change material: A numerical analysis and experimental investigation. *Int. J. Photoenergy* **2016**, *2016*, 4819675. [CrossRef]
6. Fertig, F.; Rein, S.; Schuber, M.; Warta, W. Impact of junction breakdown in multi-crystalline silicon solar cells on hot-spot formation and module performance. In Proceedings of the European Photovoltaic Solar Energy Conference and Exhibition, Hamburg, Germany, 5–6 September 2011; pp. 1168–1178.

7. Guerriero, P.; Tricoli, P.; Daliento, S. A bypass circuit for avoiding the hot spot in PV modules. *Sol. Energy* **2019**, *181*, 430–438. [CrossRef]
8. Niazi, K.A.K.; Yang, Y.; Sera, D. Review of mismatch mitigation techniques for PV modules. *IET Renew. Power Gener.* **2019**, *13*, 2035–2050. [CrossRef]
9. Al Mansur, A.; Amin, R.; Haq, M.A.U.; Maruf, H.; Mottalib, M.; Ashique, R.H.; Shihavuddin, A. Mitigation of mismatch power loss in aged photovoltaic arrays following a comparative investigation into module rearrangement techniques. *Energy Rep.* **2022**, *8*, 1896–1906. [CrossRef]
10. Dubey, R.; Chattopadhyay, S.; Kuthanazhi, V.; John, J.J.; Arora, B.M.; Kottantharayil, A.; Narasimhan, K.L.; Solanki, C.S.; Kuber, V.; Vas, J.; et al. *All-India Survey of Photovoltaic Module Degradation: Report of the National Centre for Photovoltaic (NCPRE)*; National Centre for Photovoltaic Research and Education, Indian Institute of Technology Bomba: Mumbai, India; Solar Energy Centre, National Institute of Solar Energy: Haryana, India, 2014.
11. Czanderna, A.W.; Pern, F.J. Encapsulation of PV modules using ethylene vinyl acetate copolymer as a pottant: A critical review. *Sol. Energy Mater. Sol. Cells* **1996**, *43*, 101–181. [CrossRef]
12. Pern, F.J. Factors that affect the EVA encapsulant discoloration rate upon accelerated exposure. *Sol. Energy Mater. Sol. Cells* **1996**, *41–42*, 587–615. [CrossRef]
13. Chattopadhyay, S.; Dubey, R.; Kuthanazhi, V.; John, J.J.; Solanki, C.S.; Kottantharayil, A.; Arora, B.M.; Narasimhan, K.L.; Kuber, V.; Vasi, J.; et al. Visual Degradation in Field-Aged Crystalline Silicon PV Modules in India and Correlation With Electrical Degradation. *IEEE J. Photovolt.* **2014**, *4*, 1470–1476. [CrossRef]
14. van Dyk, E.E.; Chamel, J.B.; Gxasheka, A.R. Investigation of delamination in an edge-defined film-fed growth photovoltaic module. *Sol. Energy Mater. Sol. Cells* **2005**, *88*, 403–411. [CrossRef]
15. Riedl, G.; Haselsteiner, P.; Säckl, G.; Wallner, G.M. Environmental fatigue crack growth of PV glass/EVA laminates in the melting range. *Prog. Photovolt. Res. Appl.* **2024**, *32*, 623–635. [CrossRef]
16. Li, H.Y.; Luo, Y.; Ballif, C.; Perret-Aebi, L.E. Fast and Nondestructive Detection on the EVA Gel Content in Photovoltaic Modules by Optical Reflection. *IEEE J. Photovolt.* **2015**, *5*, 759–765. [CrossRef]
17. Sinha, A.; Sastry, O.S.; Gupta, R. Nondestructive characterization of encapsulant discoloration effects in crystalline-silicon PV modules. *Sol. Energy Mater. Sol. Cells* **2016**, *155*, 234–242. [CrossRef]
18. Guerriero, P.; Codecasa, L.; d'Alessandro, V.; Daliento, S. Dynamic electro-thermal modeling of solar cells and modules. *Sol. Energy* **2019**, *179*, 326–334. [CrossRef]
19. Čabo, F.G.; Marinić-Kragić, I.; Garma, T.; Nižetić, S. Development of thermo-electrical model of photovoltaic panel under hot-spot conditions with experimental validation. *Energy* **2021**, *230*, 120785. [CrossRef]
20. Balato, M.; Botti, M.; Catalano, A.P.; Costanzo, L.; D'ALessandro, V.; Papathanasiou, A.G.; Petrarca, C.; Scognamillo, C.; Verolino, L.; Vitelli, M. Electro-Thermal Circuit Models of Photovoltaic Cells Subjected to Optical Degradation Phenomena. In *the 2025 31st International Workshop on Thermal Investigations of ICs and Systems (THERMINIC), Naples, Italy, 24–26 September 2025*; IEEE: New York, NY, USA, 2025; pp. 1–6. [CrossRef]
21. Al Mahdi, H.A.; Leahy, P.G.; Morrison, A.P. Predicting Early EVA Degradation in Photovoltaic Modules From Short Circuit Current Measurements. *IEEE J. Photovolt.* **2021**, *11*, 1188–1196. [CrossRef]
22. Muñoz, J.; Lorenzo, E.; Martínez-Moreno, F.; Marroyo, L.; García, M. An investigation into hot-spots in two large grid-connected PV plants. *Prog. Photovolt Res. Appl.* **2008**, *16*, 1062–7995. [CrossRef]
23. Deng, S.; Zhang, Z.; Ju, C.; Dong, J.; Xia, Z.; Yan, X.; Xu, T.; Xing, G. Research on hot spot risk for high-efficiency solar module. *Energy Procedia* **2017**, *130*, 77–86. [CrossRef]
24. Zhou, J.; Yi, Q.; Wang, T.; Ye, Z. Temperature distribution of photovoltaic module based on finite element simulation. *Sol. Energy* **2015**, *111*, 97–103. [CrossRef]
25. *IEC 61215-2:2021*; Terrestrial Photovoltaic (PV) Modules—Design Qualification and Type Approval—Part 2: Test Procedures. International Electrotechnical Commission: Geneva, Switzerland, 2021.
26. Castaner, L.; Silvestre, S. *Modelling Photovoltaic Systems Using PSpice*; Wiley: Chichester, UK, 2002.
27. Clugston, D.; Basore, P. PC1D Version 5: 32-bit solar cell modeling on personal computers. In Proceedings of the 26th IEEE Photovoltiac Specialists Conference, Anaheim, CA, USA, 29 September–3 October 1997; pp. 207–210.
28. Schinke, C.; Peest, P.C.; Bothe, K.; Schmidt, J.; Brendel, R.; Vogt, M.R.; Kröger, I.; Winter, S.; Schirmacher, A.; Lim, S.; et al. Experimental Determination of the Uncertainty of the Absorption Coefficient of Crystalline Silicon. *Energy Procedia* **2015**, *77*, 170–178. [CrossRef]
29. McIntosh, K.R.; Swanson, R.M.; Cotterm, J.E. A simple ray tracer to compute the optical concentration of photovoltaic modules. *Prog. Photovolt. Res. Appl.* **2006**, *14*, 167–177. [CrossRef]
30. Thomson, A.; Ernst, M.; Haedrich, I.; Quian, J. Impact of PV module configuration on energy yield under realistic conditions. *Opt. Quantum Electron.* **2017**, *49*, 82. [CrossRef]

31. Oreski, G.; Wallner, G.M. Evaluation of the aging behavior of ethylene copolymer films for solar applications under accelerated weathering conditions. *Sol. Energy* **2009**, *83*, 1040–1047. [CrossRef]
32. Balato, M.; Costanzo, L.; Vitelli, M. Series–parallel PV array reconfiguration: Maximization of the extraction of energy and much more. *Appl. Energy* **2015**, *159*, 145–160. [CrossRef]
33. Balato, M.; Costanzo, L.; Vitelli, M. Multi-objective optimization of PV arrays performances by means of the dynamical reconfiguration of PV modules connections. In Proceedings of the International Conference on Renewable Energy Research and Applications (ICRERA), Palermo, Italy, 22–25 November 2015; pp. 1646–1650. [CrossRef]
34. Kaplani, E. Detection of Degradation Effects in Field-Aged c-Si Solar Cells through IR Thermography and Digital Image Processing. *Int. J. Photoenergy* **2012**, *2012*, 396792. [CrossRef]